doi: 10.4208/cicc.2025.196.01 249 **Review**

Computational Mechanistic Insights into Non-Cubane Iron-Sulfur Cluster-Dependent Enzymes with [2Fe-2S] and [4Fe-4S] Cores: A Review

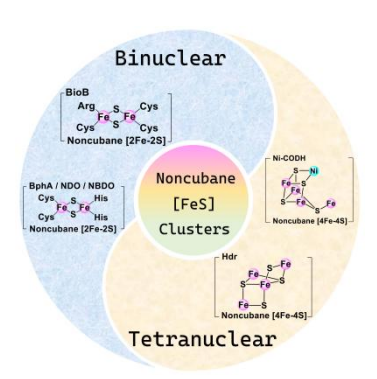
Zehan Ma and Shilu Chen*

Key Laboratory of Cluster Science of Ministry of Education, School of Chemistry and

Chemical Engineering, Beijing Institute of Technology, Beijing 100081, China.

Received on 15 July 2025; Accepted on 8 August 2025

Abstract: Iron-sulfur ([FeS]) clusters are among the most ancient and functionally diverse cofactors in biology, mediating processes ranging from electron transfer to substrate activation and catalysis. Within this broad class, non-cubane [FeS] clusters exhibit outstanding structural flexibility and chemical versatility. This review summarizes recent computational advances in elucidating the mechanisms of non-cubane [FeS] cluster-dependent enzymes, focusing on systems containing [2Fe–2S] and distorted [4Fe–4S] clusters. Representative enzymes discussed include biotin synthase (BioB), Rieske dioxygenases (NDO, BphA, NBDO), heterodisulfide reductase (Hdr), and carbon monoxide dehydrogenases (CODHs), that perform diverse chemical transformations such



as sulfur insertion, aromatic cis-dihydroxylation, S–S bond cleavage, and CO₂/CO interconversion. Special emphasis is placed on how quantum chemical cluster modelling and QM/MM simulations have provided insights into transient intermediates, rate-determining steps, and the roles of metal nuclearity and heterometal incorporation in tuning catalytic reactivity.

Key words: computational chemistry, non-cubane [FeS] cluster, metalloenzyme, reaction mechanism.

1. Introduction

Iron-sulfur ([FeS]) clusters are among the most ancient bioinorganic cofactors and have played significant roles in the evolution of cellular life [1,2]. They are essential components of a wide range of proteins and metalloenzymes, including radical *S*-adenosylmethionine (RS) enzymes [3], Rieske dioxygenase (RDOs) [4], carbon monoxide dehydrogenases (CODHs) [5], nitrogenases [6], and hydrogenases [7,8]. [FeS] clusters serve diverse functions such as electron transfer [9], catalysis [3], structural stability [10], sensor [11], and sulfur donation [12]. These versatile functional roles are closely linked to the structural diversity of [FeS] clusters. While the cubane-type [4Fe-4S] cluster has been extensively studied [13], non-cubane [FeS] clusters have attracted increasing attention for their notable conformational flexibility and high

chemical reactivity.

[FeS] clusters are composed of iron and sulfur atoms and are generally denoted as " $[m\text{Fe-}q\text{S}]^n$ ", where m, the nuclearity, represents the number of iron atoms (ranging from 2 to 18), q denotes the number of bridging sulfide ligands (typically 1 to 30), and n indicates the overall cluster charge [14]. The variability in nuclearity (m) underpins the remarkable structural diversity of [FeS] clusters, which in turn dictates their functional and reactive properties. At low nuclearity (e.g., m=2), [FeS] clusters commonly adopt nonlinear configurations in biological systems [15], such as the rhomboidal geometry of [2Fe-2S] clusters [16]. As the nuclearity increases, more complex architectures emerge, including cuboidal (m=3) [17], cubane (m=4) [18], prismatic or basket (m=6) [19], monocapped prismatic (m=7) [20], rhombic

^{*} Corresponding author: shlchen@bit.edu.cn (Shilu Chen)

dodecahedral (m = 8) [21], and edge-bridged tetracubane (m = 16) clusters [21]. Among these, the cubane-type [4Fe-4S] cluster (Figure 1.A) is the most extensively studied due to its central role in electron transfer reactions [22]. In this structure, three iron ions are typically ligated by cysteine residues from the protein, while the fourth iron serves as a binding site for an additional cysteine or other cofactors [22].

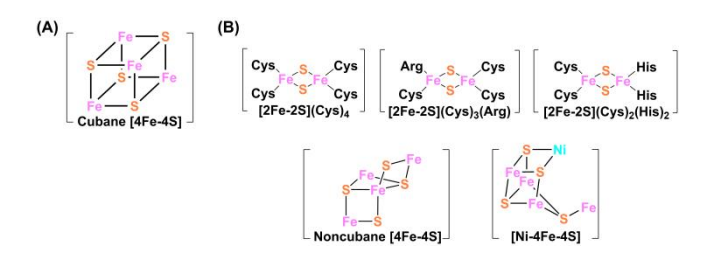


Figure 1. Structural diversity of iron–sulfur ([FeS]) clusters. (A) The canonical cubanetype [4Fe-4S] cluster. (B) Two representative non-cubane [FeS] clusters with nuclearities of 2 or 4.

Beyond the canonical cubane-type cluster, growing attention has been directed toward non-cubane [FeS] clusters in living organisms.

This expanding class of [FeS]-dependent enzymes continues to reveal novel chemical properties and biochemical functions. Recent studies have shown that non-cubane [FeS] clusters possess diverse coordination environments and pronounced structural plasticity, enabling them to participate in functions beyond electron transfer [23-26]. Due to the vast diversity of [FeS]-containing proteins and their wide-ranging biological roles, a comprehensive rationalization remains challenging. Therefore, this review focuses primarily on non-cubane [FeS] clusters with nuclearity of 2 or 4, the two most common forms (Figure 1.B) [27].

In binuclear rhomboidal configurations, the [2Fe-2S] core ligated by four conserved cysteine residues, [2Fe-2S](Cys)₄, is the predominant motif, commonly found in plant-type ferredoxins (Fd) involved in electron transport chain [28]. An unusual [2Fe-2S] configuration has also been identified in the RS enzyme superfamily [22], where the cluster features three cysteine ligands and one conserved arginine, forming [2Fe-2S](Cys)₃(Arg) [29]. This unique cluster acts as a sulfur donor during reaction [22]. Another distinct coordination pattern, [2Fe-2S](Cys)₂(His)₂, defines the Rieske-type dioxygenases, which catalyze the dihydroxylation of recalcitrant aromatic compounds [30] and hold great promise for bioremediation applications [31].

Table 1. Reactions catalyzed by non-cubane [FeS] cluster-containing enzymes.

Nuclearity	Enzyme	Reaction	[FeS] Function
2	BioB	$\begin{array}{c ccccccccccccccccccccccccccccccccccc$	Sulfur donor
	NDO	+ O ₂ NADH+H* NAD*	Electron transfer
	BphA	+ O ₂ NADH + H ⁺ NAD ⁺ BphA H H O O H	Electron transfer
	NBDO	ON NBDO NADH + H* NAD* ON NBDO ON HO OHO OHO OHO OHO OHO OHO	Electron transfer
	Hdr	$\begin{array}{cccccccccccccccccccccccccccccccccccc$	Electron transfer
4	CODHs	$CO + H_2O \longrightarrow CO_2 + 2H^+ + 2e^-$	Substrate binding/activation Electron transfer

For tetranuclear iron-sulfur clusters, a structurally distinct noncubane [4Fe-4S] cluster was identified by Shima et al. in the active site of heterodisulfide reductase (Hdr), an enzyme involved in the reduction of heterodisulfide (CoM-S-S-CoB) [32]. This cluster displays a highly distorted geometry compared to typical cubane structures [32]. Furthermore, incorporation of heterometals into [FeS] frameworks adds another layer of structural complexity, exemplified by the [Ni-4Fe-4S] cluster in CODHs [33]. Recently, a deviant enzyme termed CooS-V_{Ch} was reported, exhibiting high sequence and structural similarity to CODHs [34]. Despite sharing the typical CODHs scaffold, CooS-V_{Ch} catalyzes the reduction of hydroxylamine instead of CO oxidation or CO2 reduction. This functional switch is attributed to the redox-dependent interconversion of its active-site cluster between a reduced [4Fe-3S] form and an oxidized [4Fe-2S-S*-2O-2(H2O)] form, underscoring the remarkable evolutionary plasticity of metalloenzyme active sites. In addition, cubane-type [4Fe-4S] clusters serve as precursors to more complex metallostructures with higher nuclearities. For example, the P-cluster in nitrogenase adopts an [8Fe-7S] core, consisting of two incomplete [4Fe-3S] cubane units linked by a central hexa-coordinated sulfide (µ6-S), and is presumed to originate from the fusion of two cubane-type [4Fe-4S] clusters [14]. This unique cluster architecture plays a pivotal role in relaying electrons from the [4Fe-4S] cluster (Fe-protein) to the FeMocofactor (MoFe-protein) in nitrogenase [35]. Compared to their cubane-type counterparts, non-cubane [FeS] clusters exhibit unique evolutionary origins and structural features. In addition to their canonical roles in electron transfer, these clusters demonstrate in remarkable multifunctionality specialized chemical transformations, including substrate activation and catalysis [36].

In the studies of [FeS] cluster-containing enzymes, a range of experimental techniques were employed, including isotope labeling, kinetic analysis, and various spectroscopic methods such as electron paramagnetic resonance (EPR), Mössbauer spectroscopy, electronic absorption spectroscopy, and X-ray diffraction (XRD) [37-40]. In parallel, theoretical approaches have emerged as powerful tools for elucidating catalytic mechanisms at the molecular level. Two widely adopted computational strategies are cluster modeling [41-45] and quantum mechanics/molecular mechanics (QM/MM) hybrid method [46]. Cluster modeling focuses on the enzyme's active site and is particularly effective for investigating reaction mechanisms, while the QM/MM approach treats the active center using quantum mechanics and the surrounding protein environment using molecular mechanics. Both methods have been extensively applied across a broad range of enzymatic systems by numerous research groups [41,47-76].

Understanding the reaction mechanisms of non-cubane [FeS] cluster-dependent enzymes is of both fundamental and practical significance. In this review, we focus on the computational studies of enzymes containing non-cubane [FeS] clusters with nuclearity of 2 or 4, including biotin synthase (BioB) [29], naphthalene 1,2-dioxygenase (NDO) [77], biphenyl 2,3-dioxygenase (BphA) [78], nitrobenzene 1,2-dioxygenase (NBDO) [79], heterodisulfide reductase (Hdr) [32], and carbon monoxide dehydrogenase (CODH) [5]. The catalytic reactions facilitated by these enzymes, summarized in Table 1, include sulfur insertion [29], dihydroxylations of aromatic substrates [77-79], S-S bond cleavage [32], and CO₂/CO interconversion [5]. These enzymes are categorized into two major types based on cluster nuclearity: binuclear and tetranuclear iron-sulfur clusters. The relationship

between cluster structure and catalytic function is also discussed.

2. Methods and models

As outlined in the Introduction, two computational approaches have been developed to investigate the mechanisms of iron-sulfur cluster-dependent enzymes. The first is the quantum chemical cluster modelling, also referred to as the all-QM approach. This method involves extracting a small region of the enzyme around centered on the active site based on X-ray crystallographic data and applying high-level quantum chemical calculations to this truncated system. Over time, density functional theory (DFT) has become the preferred method for studying electronic structures of such models [80], with the B3LYP functional widely used due to its favorable balance between computational efficiency and accuracy. Advances in computational resources have allowed these cluster models to grow in size, now commonly encompassing 250-300 atoms. The surrounding protein environment is treated by considering two key effects: polarization and steric effects [81]. Polarization is accounted for using continuum solvation models with a dielectric constant of 4, simulating the electrostatic influence of the protein matrix [45]. Steric effects are addressed by employing a freezing scheme that preserves the crystallographic positions of selected atoms. Typically, the α -carbon atoms of the residues are truncated and held fixed, which maintains the structural integrity of the model while allowing flexibility in the side chains [41]. In the cluster modelling approach, both hybrid functional (e.g., B3LYP-D3 [82,83] and M06-D3 [84]) and pure functionals (e.g., BP86-D3 [85,86]) have been employed to investigate the mechanisms of the non-cubane [FeS] cluster-dependent enzymes. To achieve more accurate energetics, single-point energy calculations are performed using a high-level triple-ζ basis set, following geometry optimization with a double-ζ basis set. This approach offers distinct advantages: it can capture transient species that often inaccessible to experimental observation, and it provides detailed insights into the electronic structures and energetics essential for mechanistic

$$E_{OM/MM} = E_{OM} + E_{MM} + E_{border}$$
 (1)

The second approach is the QM/MM method, which is widely used to study the catalytic mechanisms of metalloenzymes [87-90]. This hybrid approach divides the system into two regions: an inner region (typically comprising the active site, substrates, and cofactors) treated using quantum mechanics (QM) and an outer region (comprising the surrounding protein environment and solvent) treated with molecular mechanics (MM). Commonly employed force fields for the MM region include AMBER [91], CHARMM [92], OPLS-AA [93,94], and so on. In practice, X-ray crystal structures often lack complete information, with missing amino acid residues or substrate molecules. Therefore, before constructing the computational model, it is necessary to reconstruct missing atoms, determine the protonation states of ionizable residues, and add hydrogen atoms based on estimated pK_a values, as crystallographic data typically provide coordinates only for heavy atoms. The resulting system is then solvated, and molecular dynamics (MD) simulations are carried out to equilibrate the structure and generate representative snapshots, which serve as the starting points for QM/MM calculations. It is important to note that the total QM/MM energy is not merely the sum of the individual QM and MM energies. Instead, a coupling term must be included

to account for interactions at the boundary between the QM and MM regions, as described in the equation (1) [95].

Currently, both computational approaches, cluster modelling and QM/MM, are being extended to increasingly complex systems. For example, cluster models now frequently exceed 300 atoms, and QM regions in QM/MM simulations are growing larger [13]. As a result, the outcomes of these two methodologies are gradually converging in terms of accuracy and applicability.

3. Non-Cubane binuclear Iron-Sulfur clusters

3.1 Biotin synthase (BioB)

Biotin synthase (BioB), encoded by the *BioB* gene, is a member of the radical *S*-adenosylmethionine (SAM) superfamily of enzymes [22]. BioB catalyzes the final step in biotin biosynthesis, inserting sulfur atoms into the desthiobiotin (DTB) precursor at the C⁶ and C⁹ carbon positions (Table 1) [29]. In nearly all organisms, the resulting product, biotin, functions as an essential cofactor in enzymatic carboxylation, decarboxylation, and transcarboxylation

reactions [96,97].

The BioB from Escherichia coli was among the earliest members of radical SAM enzymes to be structurally characterized by X-ray crystallography [22] (PDB: 1r30), as reported by Drennan and co-workers in 2004 [29]. The crystal structure, resolved at 3.4 Å, reveals BioB as a homodimer provides detailed insight into its the active site, including the bound substrate, key cofactors, and essential amino acid residues [29]. In the active site, BioB contains the family-defining radical SAM [4Fe-4S]_{RS} cluster, coordinated by the conserved CX_3CX_2C motif (C = Cys; X = any amino acid) [22]. Like most radical SAM enzymes [22], BioB utilizes the reduced [4Fe-4S]_{RS} cluster to donate one electron to SAM, initiating homolytic cleavage of the S-C5' bond. This reductive cleavage of SAM generates methionine and a highly reactive 5'-deoxyadenosyl radical (5'-dAdo') (Scheme 1), which abstracts a hydrogen atom from the substrate to drive catalysis. The activation barrier of the S-C^{5'} bond cleavage is calculated to be 16.0 kcal mol⁻¹ at the QM (B3LYP/SV(P))/MM (CHARMM) level of theory [98].

Scheme 1. A typical radical SAM reaction. SAM: S-adenosylmethionine. Energy barrier (in kcal mol⁻¹) calculated in the BioB enzyme is given.

In addition to the $[4\text{Fe-4S}]_{Rs}^+$ cluster, BioB possesses an auxiliary $[2\text{Fe-2S}]_{Aux}^{2+}$ cluster coordinated by four conserved residues (Cys97, Cys128, Cys188, and Arg260) as shown in Figure 2. Despite the unusual presence of an arginine ligand, Broach and Jarrett demonstrated that Arg260 is not essential for BioB activity in vitro or in vivo [99]. It has been proposed that Arg260 may play an electronic, structural, or mechanistic role, potentially related to its bidentate coordination or its charged state upon protonated [99,100].

The substrate, desthiobiotin (DTB), is positioned between SAM and the [2Fe-2S]_{Aux} cluster. The C^9 and C^6 carbons of DTB are located 3.9 Å and 4.1 Å, respectively, from the $C^{5'}$ of SAM [29]. Notably, the shortest distance between a bridging sulfide of the [2Fe-2S]_{Aux} cluster and the C^9 atom is only 4.6 Å, suggesting a direct role for the [2Fe-2S]_{Aux} cluster in facilitating C-S bond formation.

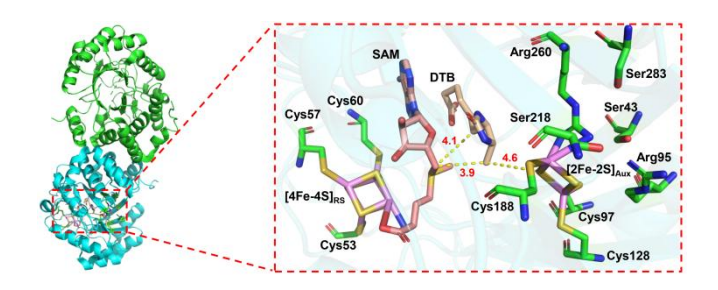


Figure 2. Crystal structure of biotin synthase (BioB) and its active site (PDB: 1r30) [29].

In 2010, due to the limited resolution of the available crystal

structure, Ryde and co-workers performed both QM/MM calculations and quantum refinement to investigate the structural properties of BioB [100]. Their QM/MM results indicated that the Arg260 ligand is deprotonated and coordinates to the iron center via its NH group, rather than NH₂. Moreover, quantum refinement revealed a significantly shorter Fe-Fe distance within the [2Fe-2S]_{Aux} cluster (approximately 2.7 Å) compared to the 3.3 Å observed in the crystal structure, suggesting that the crystallographic model may reflect a mixture of redox states or be distorted due to low resolution. The study concluded that more accurate structural data, complemented by advanced theoretical investigations, are required to fully elucidate the enzymatic mechanism.

Scheme 2. Proposed reaction mechanism for BioB [100].

Although current theoretical studies of BioB's catalytic mechanism remain constrained by the resolution of its structural data, a widely accepted mechanistic proposal is summarized in Scheme 2. Upon formation of the 5'-dAdo' radical, the first hydrogen abstraction occurs at the C⁹ position of DTB, generating a C⁹-dethiobiotinyl radical. This methylene radical subsequently forms a C-S bond with a bridging sulfide from the [2Fe-2S]_{Aux} cluster, producing a stable 9-mercaptodethiobiotin (MDTB) intermediate [22]. Completion of the biotin molecule requires a second SAM molecule to abstract a hydrogen from the C⁶ position of DTB. The resulting C⁶-centered radical undergoes a second C-S bond-forming reaction with the same auxiliary sulfide in the [2Fe-2S]_{Aux} cluster, ultimately yielding biotin.



Figure 3. Electron transport chain in the multicomponent Rieske dioxygenases (RDOs).

The origin of the sulfur atom in biotin synthesis has long been a subject of investigation. A growing body of experimental evidence [101-103] supports the role of the [2Fe-2S]_{Aux} cluster as the direct sulfur donor in this transformation. As shown in Scheme 2, it is now widely accepted that the [2Fe-2S]_{Aux} cluster donates one of its bridging sulfides during catalysis, effectively sacrificing itself in the process. To achieve multiple catalytic turnovers, Jarrett and coworkers proposed that Fe-S cluster biosynthesis systems such as ISC or SUF regenerate the [2Fe-2S]_{Aux} cluster *in vivo*, thereby maintaining catalytic efficiency [29]. Future high-resolution structural data and advanced computational studies will be essential for deepening the understanding of the BioB catalytic mechanism.

3.2 Rieske dioxygenases (RDOs)

Rieske dioxygenases (RDOs) are non-heme iron-dependent enzymes that play crucial roles in the bioremediation of polluted environment [31]. The currently known RDOs primarily catalyze the initial step in the degradation of aromatic compounds via regioand stereospecific cis-dihydroxylation, producing dihydrodiols. The RDO family is characterized as a multi-component enzyme system composed of an oxygenase, a reductase, and a ferredoxin [104,105]. The oxygenase component carries out the catalytic function and contains both a Rieske-type [2Fe-2S] center and a non-heme mononuclear iron center [104]. The reductase and ferredoxin components form the electron transport chain (ETC) [104], which includes plant-type [2Fe-2S] clusters and Rieske-type [2Fe-2S] clusters, respectively (Figure 3). The specific roles of these rhombic [2Fe-2S] clusters within the RDO system will be discussed in detail in the following sections.

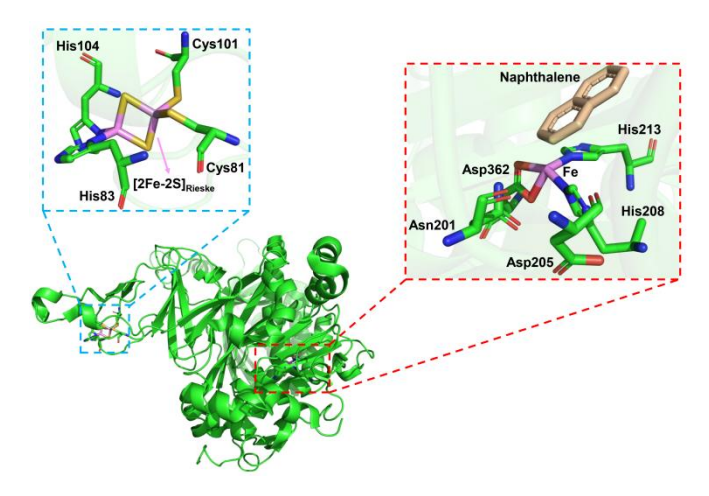


Figure 4. Crystal structure of naphthalene 1,2-dioxygenase (NDO) and its active site (PDB: 107G) [77].

3.2.1 Naphthalene 1,2-dioxygenase (NDO)

Naphthalene 1,2-dioxygenase (NDO) is one of the most extensively studied RDOs. It initiates the catabolism of naphthalene by converting it into *cis*-dihydrodiol (Table 1). The crystal structure of NDO (PDB: 107G) was resolved by Ramaswamy's group in 2003 (Figure 4) [77]. The reaction mechanism of NDO involves five key steps (Scheme 3). Initially, an additional electron is preferentially transferred to the iron atom coordinated by two histidines in the [2Fe-2S]_{Rieske} cluster [104]. Upon binding of O₂ and H⁺, a reactive Fe^{III}-OOH species is formed, marking the onset of dioxygen activation. To elucidate the preferred reaction pathway, the subsequent steps following the substrate attacked by Fe(III)-OOH have been investigated by theoretical calculations.

$$\begin{array}{c} \text{Cys} \\ \text{Cys} \\ \text{Cys} \\ \text{S} \end{array} \\ \text{Fe}^{3+} \\ \text{S} \end{array} \\ \text{Fe}^{3+} \\ \text{His} \\ \text{Fe}^{3+} \\ \text{Cys} \\ \text{His} \\ \text{Fe}^{3+} \\ \text{Cys} \\ \text{His} \\ \text{Fe}^{3+} \\ \text{Cys} \\ \text{His} \\ \text{Fe}^{3+} \\ \text{OH} \\ \text{OH}$$

Scheme 3. Proposed mechanism of aromatic cis-dihydroxylation catalyzed by NDO [104,105]. Energy barrier is given in keal mol⁻¹.

In 2004, Siegbahn and co-workers performed DFT calculations to figure out the reaction mechanism of NDO, using a chemical model derived from the crystal structure [104,105]. Their study proposed a concerted mechanism, as illustrated in Scheme 3. The calculations indicate that the Fe^{III}-OOH species oxidizes the substrate directly via an epoxide intermediate. This involves heterolytic cleavage of the O-O bond in the Fe^{III}-OOH hydroperoxo ligand, concurrent with the formation of two new C-O bonds. This step constitutes the rate-limiting stage of the reaction, with an associated energy barrier of 17.5 kcal mol-1. Following epoxide ring opening, the resulting carbocation is attacked by the hydroxy ligand, leading to the formation of cis-dihydrodiol. They also examined the possibility of an alternative pathway involving the formation of a high-valent iron(V)-oxo species (HO-Fe^V=O) prior to substrate hydroxylation. However, this route was ruled out due to the significantly higher energy barrier for O-O bond cleavage (26.5 kcal mol⁻¹).

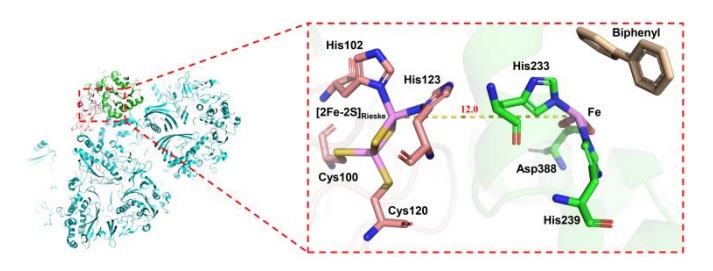


Figure 5. Crystal structure of biphenyl 2,3-dioxygenase (BphA) and its active site (PDB: 5aew) [78].

In 2014, Pappalardo and co-workers conducted MD and docking simulations to explore NDO mutants with high degradation capabilities [106]. They modeled eleven NDO variants, focusing on modifications to the active site cavity to better accommodate high-molecular-weight polycyclic aromatic hydrocarbons (PAHs), while preserving the enzyme's hydrophobic and electrostatic properties. MD trajectories (20 ns per mutant) confirmed structural stability, with secondary structure deviations remaining below 5% relative to wild-type NDO. Docking studies revealed that mutants with expanded active site volume exhibited favorable interactions with

bulky PAHs. This study provides valuable insights for the rational design of more effective bioremediation enzymes and highlights the potential of computational approaches to guide experimental optimization under extreme environmental conditions.

In 2022, Reiher and co-workers further investigated the role of the substrate in the catalytic cycle of RDOs using a combination of quantum chemical methods, including DFT, coupled cluster (DLPNO-CCSD(T)), and CASSCF calculations [107]. Using NDO as a model system, they systematically evaluated the influence of substrate binding on key elementary steps involved in O₂ activation. Specifically, they examined the transition of the non-heme Fe^{II} center from a hexa- to penta-coordinate state, O₂ binding, and electron transfer from the Rieske cluster. Their results indicate that while substrate presence does not significantly affect the initial stages of O₂ activation, it plays a crucial role after oxidation of the Rieske cluster, facilitating electron transfer and promoting O₂ activation through allosteric control. The findings suggest strategies for optimizing biocatalysts for environmental pollutant degradation by enhancing substrate-mediated activation pathways.

3.2.2 Biphenyl 2,3-dioxygenase (BphA)

Biphenyl and its chlorinated derivatives, such as polychlorinated biphenyls (PCBs), are persistent organic pollutants with serious environmental and health consequences [108]. Extensive efforts have been devoted to investigate their toxicological effects and environmental behavior. Among various remediation strategies, biodegradation has attracted growing attention due to its environmental sustainability and cost-effectiveness. The aerobic degradation of biphenyl and PCBs is proposed to involve four key enzymes, including biphenyl 2,3-dioxygenase (BphA), cis-2,3dihydro-2,3-dihydroxybiphenyl dehydrogenase (BphB), 2,3dihydroxybiphenyl 1,2-dioxygenase (BphC), and 2-dydroxy-6phenyl-6-oxohexa-2,4-dienoate hydrolase (BphD) [109,110]. Among these, BphA catalyzes the initial step in the aerobic degradation pathway of biphenyl and PCBs (Table 1). BphA is a prototypical RDO enzyme composed of three components: an oxygenase, a ferredoxin, and a reductase. The crystal structure of BphA (PDB: 5aew), determined by Kumar and co-workers in 2016 [78], provides a valuable structural framework for subsequent mechanistic and computational investigations.

$$\begin{array}{c} \text{Cys} \\ \text{Fe}^{3+} \\ \text{Cys} \\ \text{S} \\ \text{Fe}^{3+} \\ \text{S} \\ \text{Fe}^{3+} \\ \text{S} \\ \text{Fe}^{3+} \\ \text{S} \\ \text{Fe}^{3+} \\ \text{His} \\ \text{OH} \\ \text{H}^{+}/\text{e}^{-} \\ \end{array}$$

Scheme 4. Proposed mechanism of aromatic cis-dihydroxylation catalyzed by BphA [108]. Energy barrier is given in kcal mol⁻¹.

In 2020, Zhang and co-workers employed a QM/MM approach to elucidate the BphA-catalyzed *cis*-dihydroxylation pathway of biphenyl and 4,4'-dichlorobiphenyl [108]. Due to the absence of

substrate in the original crystal structure, they utilized MD simulations and molecular docking to model the binding conformations of biphenyl-hydroperoxo-iron(III) complexes and

PCB-hydroperoxo-iron(III) complexes. The QM/MM model comprised a QM region containing the substrate, the hydroperoxoiron(III) species, and key coordinating residues, while the MM region represented the surrounding protein environment. Like NDO, the reaction mechanism of BphA mainly involves formation of an epoxide intermediate, conversion to a carbocation species, and final hydroxylation yielding the cis-diol products (Scheme 4). The ratedetermining epoxide formation exhibited energy barriers of 17.6 kcal mol-1 for biphenyl and 19.8 kcal mol-1 for 4,4'dichlorobiphenyl, consistent with experimental data [111]. Electrostatic interaction analysis identified key residues involved in modulating catalytic efficiency, highlighting their roles in substrate binding and transition-state stabilization. These findings suggested potential targets for future site-directed mutagenesis. Notably, chlorine substitution in PCBs slightly increased the reaction barrier, indicating substrate-dependent catalytic challenges. This study underscores the utility of QM/MM in deciphering enzyme mechanisms difficult to access experimentally and provides actionable insights for engineering BphA variants with enhanced PCB-degrading capabilities. These findings contribute to advancing bioremediation strategies for the removal of persistent environmental contaminants.

3.2.3 Nitrobenzene 1,2-dioxygenase (NBDO)

Nitroaromatic compounds are widely utilized in industrial processes, including pharmaceutical synthesis, dye production, and explosives manufacturing [112]. However, many of these compounds are toxic and carcinogenic, and persist as recalcitrant environmental pollutants [112]. An effective strategy for their degradation involves the use of bacteria isolated from nitroarene-contaminated environments. In the *Comamonas* sp. JS765 strain, nitrobenzene is converted into *cis*-diol product, catalyzed by nitrobenzene 1,2-dioxygenase (NBDO) (Table 1) [79]. In 2005, Friemann and co-workers resolved the crystal structure of NBDO (PDB: 2BMQ) [79] (Figure 6), revealing a hetero-hexameric architecture characteristic of the RDO family.

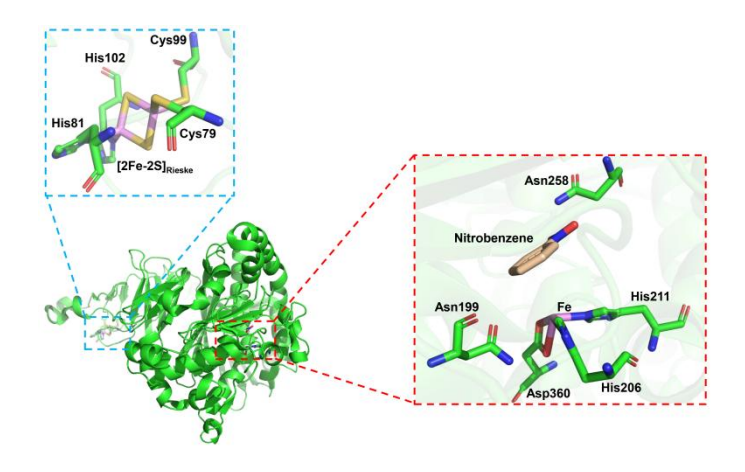


Figure 6. Crystal structure of nitrobenzene 1,2-dioxygenase (NBDO) and its active site (PDB: 2BMQ) [79].

In 2014, Paneth and co-workers employed DFT calculations to investigate the mechanism of nitrobenzene *cis*-dihydroxylation catalyzed by NBDO [113]. The chemical models were built based on the crystal structure of NBDO with the substrate bound in the active site. Four models of varying size were constructed to explore both concerted and stepwise mechanisms. The results indicated that

formation of the high-valent iron(V)-oxo species (HO-Fe^V=O) is energetically favorable and likely precedes substrate oxidation. This species arises via heterolytic cleavage of the O-O bond in the ferric hydroperoxo intermediate (Fe^{III}-OOH). The calculated Gibbs free energy barriers for this step ranged from 14.6 to 16.7 kcal mol $^{\rm l}$, depending on the model, supporting its feasibility in the enzymatic context.

Paneth et al.'s study [113] evaluated potential reaction pathways initiated by either the HO-Fe^V=O or Fe^{III}-OOH species attacking the aromatic ring. Three potential pathways for substrate oxidation by HO-Fe^V=O were considered, including the attack of the hydroxyl on the C² atom, and the attack of the second oxygen of the hydroperoxo on either the C¹ or C² atoms (Figure 7). The most plausible pathway involves initial hydroxyl attack on the C² position, generating a substrate radical that ultimately leads to the formation of the *cis*-dihydrodiol product (Scheme 5). This mechanism aligns with experimental ¹⁸O-labeling studies, which confirm incorporation of oxygen into the product [114].

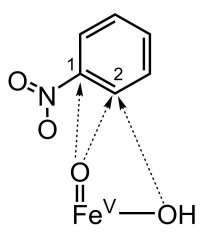


Figure 7. Three proposed pathways for the initial attack of HO- Fe^{V} =O on the substrate during the *cis*-dihydroxylation reaction catalyzed by NBDO.

Alternative mechanisms involving direct attack of the Fe^{III}-OOH intermediate on the aromatic ring were also explored by Paneth et al [113]. These include both concerted and stepwise pathways targeting the C-C double bond to form epoxide intermediates. However, these pathways were found to be less favorable than the mechanism mediated by HO-Fe^V=O. The calculated activation barriers for epoxide formation were significantly higher, ranging from 20.6 to 38.7 kcal mol⁻¹, depending on the model and specific site of attack. Moreover, unlike in the NDO enzyme, the resulting epoxide intermediates in NBDO were dissociated from the mononuclear iron center, with extended distances between the arene oxide and the iron atom, likely preventing subsequent transformation to the final *cis*-dihydrodiol product.

Despite the high sequence similarity between NBDO and NDO, their reaction mechanisms differ significantly. In NDO, the formation of an epoxide intermediate is a plausible step toward product formation. In contrast, for NBDO, the epoxide intermediate is unstable and does not progress to the final product. This divergence is attributed to the nitro substituent in NBDO substrates, which affects the stability of the intermediates and alters the reaction pathway. These findings highlight the importance of mechanistic insights into NBDO-catalyzed transformations for advancing bioremediation strategies.

It can be seen that Rieske-type iron-sulfur clusters play a crucial role in transferring electrons to the mononuclear iron active center. Different research groups employed a variety of theoretical approaches to investigate the catalytic mechanisms of RDOs. Both cluster modelling and QM/MM approaches have proven effective in identifying key intermediates, short-lived radicals, transition

states, and dynamic changes in iron-sulfur clusters throughout the reaction cycle. The mechanistic diversity among RDO family members can largely be attributed to differences in substrate structure, which can be broadly categorized into non-substituted aromatic compounds and substituted aromatic compounds. NDO and BphA catalyze reactions involving non-substituted aromatics and typically proceed via epoxide intermediates, whereas NBDO

acts on substituted aromatics, following a distinct pathway that involves the formation of a high-valent iron(V)-oxo species (HO-Fe V =O). In addition, while Rieske-type [2Fe-2S] clusters are well established as initial electron donors to the catalytic center, their potential role in subsequent stages of the reaction remain an intriguing area for further investigation.

$$\begin{array}{c} \text{Cys} \\ \text{Cys} \\ \text{Cys} \\ \text{S} \end{array} \\ \text{Fe}^{3+} \\ \text{S} \end{array} \\ \text{Fe}^{3+} \\ \text{His} \end{array} + \begin{array}{c} \text{Fe}^{2+} \\ \text{Fe}^{3+} \\ \text{Cys} \\ \text{S} \end{array} \\ \text{Fe}^{3+} \\ \text{Cys} \\ \text{Cys} \\ \text{S} \end{array} \\ \text{Fe}^{3+} \\ \text{Cys} \\ \text{Cys} \\ \text{S} \end{array} \\ \text{Fe}^{3+} \\ \text{Cys} \\ \text{Cys} \\ \text{S} \end{array} \\ \text{Fe}^{3+} \\ \text{Cys} \\ \text{Cy$$

Scheme 5. Proposed reaction mechanism for NBDO based on DFT calculations [113]. Energy barrier is given in kcal mol⁻¹.

4. Non-cubane tetranuclear Iron-Sulfur clusters

4.1 Heterodisulfide reductase (Hdr)

Heterodisulfide reductase (Hdr) is a key enzyme in the Wolfe cycle of methanogenic archaea, responsible for the reduction of heterodisulfide (CoM-S-S-CoB) to coenzyme M (CoM-SH) and coenzyme B (CoB-SH) (Table 1) [115,116]. This reaction is essential for methane production from CO₂ and H₂, a process central to the global carbon cycle [117].

The crystal structure of Hdr reveals the presence of two noncubane [4Fe-4S] clusters (HB1 and HB2) in its active site [32]. Unlike the common cubane [4Fe-4S] clusters, these non-cubane clusters possess a distinct architecture consisting of interconnected [3Fe-4S] and [2Fe-2S] subunits that share one Fe and one S atom. This unusual structural arrangement is stabilized by five cysteine ligands per cluster, i.e., Cys153, Cys193, Cys194, Cys231, and Cys234 for HB1, while Cys9, Cys41, Cys42, Cys78, and Cys81 for HB2 (Figure 8).

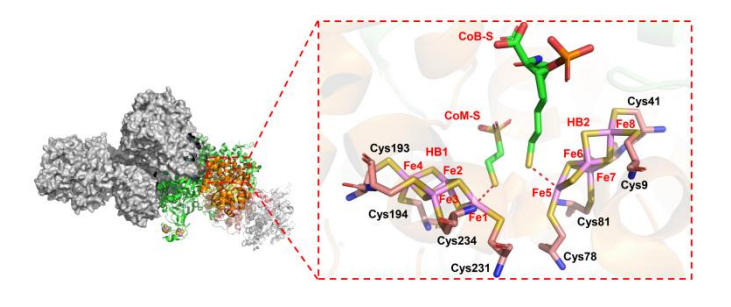


Figure 7. Crystal structure of heterodisulfide reductase (Hdr) and its active site (PDB: 5ODR) [32].

Recently, Chen and co-workers used DFT calculations to investigate the detailed mechanism of Hdr-catalyzed reduction of CoM-S-S-CoB [118]. They proposed three possible pathways,

classified according to the initial addition of proton/electron pairs (H⁺/e⁻) to the enzyme-substrate complex. Under H⁺/e⁻-deficient conditions, characterized by slow proton-coupled electron transfer (PCET), the Hdr reaction starts with the S-S bond cleavage of CoM-S-S-CoB, facilitated by two [4Fe-4S]²⁺ clusters (mechanism A in Scheme 6). This step has an energy barrier of 18.7 kcal mol⁻¹ and is identified as rate-limiting. The resulting intermediates, HB1 [4Fe-4S]³⁺-S-CoM and HB2 [4Fe-4S]³⁺-S-CoB, are subsequently reduced through two PCET process, ultimately yielding the coenzymes M and B. Meanwhile, the two [4Fe-4S]³⁺ clusters are regenerated to their original [4Fe-4S]²⁺ state.

Under H^+/e^- -sufficient conditions, characterized by fast PCET), the Hdr reaction preferentially proceeds via the addition of either one (mechanism B summarized in Scheme 6) or two pairs of H^+/e^- (mechanism C in Scheme 6) to the active site.

In Mechanism B, the initial addition of one pair of H⁺/e⁻ to the enzyme-substrate complex leads to reduction of the HB1 [4Fe-4S]2+ cluster to [4Fe-4S]+, accompanied by protonation of the sulfur atom of Cys234. Consequently, the two clusters adopt different oxidation states (HB1: [4Fe-4S]⁺; HB2: [4Fe-4S]²⁺). Protonation of Cys234 disrupts its coordination with Fe1, inducing a significant geometric distortion in the HB1 cluster, , as evidenced by an increase in the Fe1-S2-Fe3 bond angle from 79.4° to 99.2°. From this intermediate, featuring neutral cysteine (Cys234-H), the proton can be transferred either to the Cys231 sulfur (mechanism B- α) or to the S1 sulfur of HB1 (mechanism B- β). Mechanism B- α is characterized by a low barrier, indicating a rapid proton transfer. Mechanism B-β involves a slightly higher but still favorable activation barrier of 4.7 kcal mol⁻¹ and a slight exothermicity of 3.0 kcal mol-1. The next step involves cleavage of the S-S bond in CoM-S-S-CoB, with a barrier of 8.7 kcal mol⁻¹ and an exothermicity of 3.3 kcal mol-1. This barrier is readily surmountable and represents the rate-determining step in the pathway where the proton is transferred from Cys234 to Cys231 (mechanism B-α). In mechanism B-β, S-S bond dissociation

proceeds with a slightly higher barrier of 11.1 kcal mol-1, suggesting that protonation of the HB1 cluster helps maintain its catalytic activity during this critical step. Importantly, in both pathways, S-S bond dissociation following the addition of a single H⁺/e⁻ pair exhibits lower energy barriers than in mechanism A (18.7) kcal mol-1), indicating that formation of a monovalent non-cubane cluster facilitates disulfide bond dissociation. Subsequently, in mechanism B-a, the proton from Cys231 is transferred to the sulfur atom of the CoB-S- fragment, with an energy barrier of 3.3 kcal mol⁻¹ and an exothermicity of 3.3 kcal mol⁻¹. Finally, another pair of H⁺/e⁻ is delivered to the CoM-S⁻ fragment, forming CoM-SH and regenerating the HB1 [4Fe-4S]²⁺ cluster from its oxidized [4Fe-4S]²⁺ state. In the B-β pathway, following S-S bond cleavage, a proton is transferred from the HB1 S1 atom to the sulfur of coenzyme M, also accompanied by another H⁺/e⁻ pair addition. Overall, mechanism B illustrates the enzyme's ability to utilize available proton-electron pairs to reduce activation barriers and accelerate the reaction rate, highlighting the functional versatility and redox adaptability of the non-cubane [4Fe-4S] cluster in facilitating catalysis.

In competing mechanism C, the reaction begins with two PCET events, leading to the reduction of both [4Fe-4S]²⁺ clusters. Simultaneously, protons are added to Cys234 and the HB1 cluster, respectively. The proton on Cys234 is then transferred to Cys231,

with an energy barrier of 5.0 kcal mol⁻¹. This is followed by cleavage of the S-S bond, which proceeds with a barrier of 4.4 kcal mol⁻¹, suggesting that the S-S bond dissociation is more energetically accessible under conditions involving two PCET events. Finally, product formation occurs via two proton transfer processes: one proton is transferred from Cys231 to CoB-S⁻, forming CoB-SH, and the other from the HB1 cluster to CoM-S⁻, yielding CoM-SH.

The overall barriers in mechanisms B and C are lower than that in mechanism A (18.7 kcal mol⁻¹), suggesting that although mechanism A is feasible, it becomes less favorable under conditions of efficient PCET.

Comparison of these mechanistic pathways reveals the unique catalytic properties of non-cubane [4Fe-4S] clusters. These clusters exhibit greater geometric flexibility and enhanced reactivity compared to the classic cubane [4Fe-4S] cluster. Notably, the monovalent [4Fe-4S]⁺ cluster displays higher activity than the divalent [4Fe-4S]²⁺ form in promoting S-S bond dissociation in CoM-S-S-CoB. This detailed mechanistic investigation underscores the critical role of non-cubane iron–sulfur clusters in catalysis and highlights their evolutionary adaptation toward facilitating challenging chemical transformations, such as S-S bond cleavage, through their highly distorted architectures.

Scheme 6. Proposed reaction mechanisms for the S-S bond dissociation catalyzed by Hdr under different oxidation states of non-cubane [4Fe-4S] clusters: (A) Two [4Fe-4S]²⁺ clusters; (B) one [4Fe-4S]¹⁺ and one [4Fe-4S]²⁺ cluster; (C) two [4Fe-4S]¹⁺ clusters. Energy barriers are given in kcal mol⁻¹.

4.2 Carbon monoxide dehydrogenases (CODHs)

The structural and functional evolution of tetranuclear non-cubane iron-sulfur clusters has become a cornerstone in the understanding of biological redox catalysis. Undoped non-cubane [4Fe-4S] clusters, typified by distorted geometries and asymmetric ligand coordination, exhibit remarkable electronic flexibility that supports their roles within enzymes. However, their catalytic capacity is often limited by the redox properties of the single-metal center. The introduction of heterometals (e.g., Mo, V, or Ni) into an iron-sulfur frameworks represents a significant advancement in bioinorganic catalysis [14]. A representative example of this evolutionary innovation is found in the nickel-containing carbon monoxide (CODHs), which feature dehydrogenases tetranuclear iron-sulfur clusters.

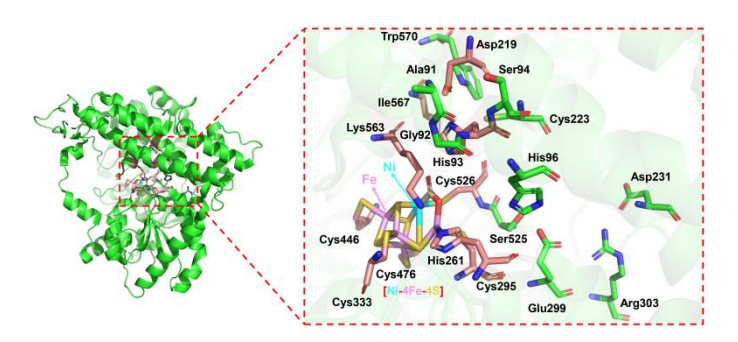
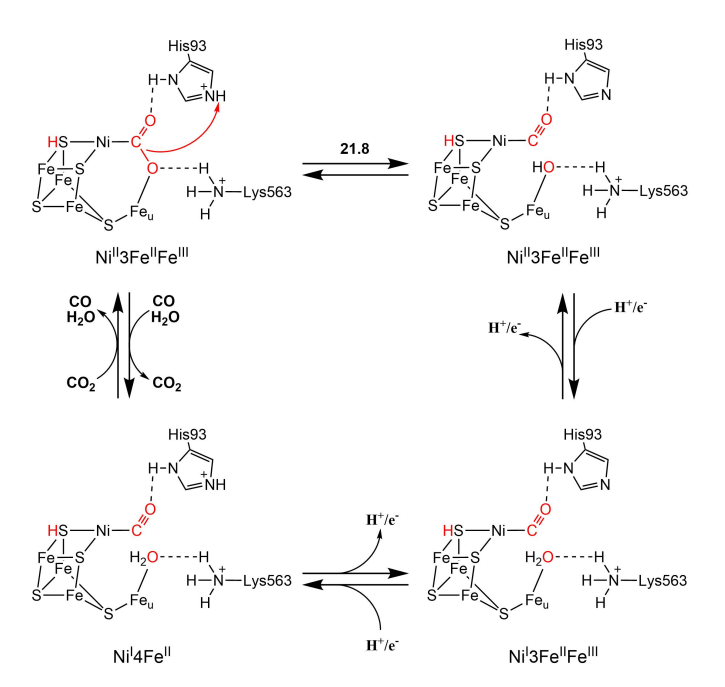


Figure 8. Crystal structure of nickel-containing carbon monoxide dehydrogenase (Ni-CODH) and its active site (PDB: 3B52) [4].



Scheme 7. Proposed mechanism for the reversible reduction of CO₂ to CO by Ni-CODH, based on DFT calculations [125]. Energy barrier is given in kcal mol⁻¹.

CODHs are enzymes that catalyze the reversible reduction of CO₂ to CO (Table 1), a reaction of fundamental importance in microbial metabolism and global carbon cycling [119]. CODHs can be divided into two types [120]: (i) Ni-CODH, which contains a tetranuclear metal cluster, and (ii) Mo/Cu-CODHs [121]. This review focuses primarily on Ni-CODH, which feature a non-

cubane iron-sulfur cluster at the active site. The atypical active site in Ni-CODH, known as the C-cluster ([Ni-4Fe-4S]), consists of a [Ni-3Fe-4S] unit along with an unusual iron atom positioned outside the cubane framework. Identified by Mössbauer spectroscopy as a ferrous component II (FCII), This extra iron, also referred to as the unique iron (Fe_u) or pendant Fe, is bridged to the cluster via a sulfide ligand [122].

In 2011, Amara and co-workers used QM/MM calculations to study the mechanism of Ni-CODH [123]. This enzyme functions through multiple redox states, with the C_{red1} and C_{red2} states being particularly well-studied. The C_{red1} state, characterized by a distinctive EPR signal, is proposed to contain a bridging hydroxide ligand between Ni^{II} and Fe_u. This state is crucial for the initial binding of CO, which is subsequently oxidized to CO_2 . In addition, the more reduced C_{red2} state, involving two additional electrons, is suggested to include a Ni-H species within the catalytic cycle.

In 2015, Dobbek and co-workers employed DFT calculations to elucidate how CO2 binds to and is activated by the C-cluster [124]. They study revealed the electronic and geometric changes accompanying CO₂ coordination. The results emphasize the critical role of a strongly nucleophilic Ni center in the C_{red2} state, whose finely tuned electronic structure facilitates CO2 reductive activation and stabilizes the two-electron-reduced intermediate via π backbonding interactions. The geometry of bound CO2 significantly deviates from that of free CO2, exhibiting elongated C=O bonds and a bent configuration. The O-C-O bond angle was measured at 117.8°, markedly reduced from the linear geometry of free CO2. These findings underscore the unique electronic and structural features of the [Ni-4Fe-4S] cluster that enable efficient CO₂ activation, reflecting a "bifunctional catalysis" mechanism involving a juxtaposed electrophilic Fe center and a nucleophilic Ni center.

In 2019, Liao and co-workers employed a quantum-chemical cluster modelling method to further investigate the reaction mechanism of Ni-CODH [125]. The model was built based on the X-ray crystal structure (PDB: 3b52), with CO₂ bound in the active site [4]. Their calculations indicate that the catalytic cycle of CO₂ reduction by Ni-CODH comprises several key steps, including CO2 binding, C-O bond cleavage, and successive reduction steps (Scheme 7). Initial CO₂ binding at the Ni site of the [Ni-4Fe-4S] cluster is stabilized by hydrogen bonding interactions from nearby residues such as Lys563 and His93. The C-O bond cleavage, a crucial mechanistic step, was calculated to have an energy barrier of 21.8 kcal mol⁻¹, aligning reasonably with experimental rate measurements (~ 18.0 kcal mol⁻¹) [126,127]. This step yields an intermediate featuring a CO molecule bound to Ni and a hydroxide ion coordinated to Feu. The first reduction involves the transfer of one electron and one proton, producing water and a Ni(I) state. The second electron/proton transfer results in a Ni(I) center accompanied by a protonated Asp219-His93 pair, with an endothermicity of 2.7 kcal mol⁻¹. Overall, the CO₂ reduction process is nearly thermoneutral, with a net energy change of only 0.6 kcal mol⁻¹. CO oxidation, the reverse of CO₂ reduction, is a critical part of the enzyme's catalytic cycle and is experimentally observed to proceed more rapidly than CO2 reduction, consistent with Liao et al.'s theoretical results. The proposed mechanism for CO oxidation mirrors the CO2 reduction pathway, reinforcing the overall reversibility and mechanistic symmetry of the catalytic cycle. Liao et al.'s study also assessed the reliability of various DFT functionals by adjusting the proportion of exact exchange,

determining that 15% provided the most accurate results.

In 2021, Greco and co-workers also employed DFT calculations to investigate the mechanism of CO_2 binding and release at the C-cluster, using an expanded cluster model [128]. Their study emphasized the critical role of the protein environment in modulating the reaction pathway. Notably, they found that the protonation state of His93 significantly affects the direction of the CO_2/CO interconversion. When His93 is protonated, CO_2 binding is energetically favored. Additionally, their calculations revealed that the redox state of the C-cluster strongly influences the energetics of CO_2 binding and dissociation. The most plausible pathway begins with the C_{red2} state, in which CO_2 bridges the Ni and Fe_u ions.

Collectively, these findings demonstrate that incorporation of Ni into tetranuclear non-cubane iron-sulfur cluster expands their catalytic capabilities by enabling substrate binding and activation. This functional diversification through heterometal incorporation highlights the evolutionary significance of metal doping in expanding the reactivity of [FeS] cluster-based cofactors.

5. Summary and outlook

In this review, we have systematically examined recent computational advances in elucidating the catalytic mechanisms of non-cubane iron-sulfur ([FeS]) cluster-dependent enzymes. These clusters, characterized by their extensive range of nuclearity and diverse coordination environments, exhibit remarkable structural plasticity and chemical versatility that enable a wide array of biological functions. Focusing on two major structural forms, [2Fe-2S] and non-cubane [4Fe-4S]) clusters, we highlighted representative enzymatic systems and how theoretical studies have deepened our mechanistic understanding.

Binuclear [2Fe-2S] clusters, which often adopt planar or rhomboidal geometries, are exemplified by enzymes such as biotin synthase (BioB) and the Rieske dioxygenases (RDOs). These clusters exhibit coordination variability, including (Cys)4, (Cys)2(His)2, and (Cys)3(Arg) motifs, and are involved in functions ranging from electron transfer to substrate hydroxylation and sulfur atom donation. Computational studies have successfully captured key reactive intermediates and helped elucidate how subtle differences in coordination environment and substrate identity influence reactivity and selectivity.

Non-cubane tetranuclear [4Fe-4S] clusters exhibit threedimensional architectures with enhanced conformational flexibility. representative enzymes were discussed, heterodisulfide reductase (Hdr), which contains highly distorted [4Fe-4S] clusters, and carbon monoxide dehydrogenase (CODH), which features a heterometal-doped ironsulfur cluster, the [Ni-4Fe-4S] C-cluster. These systems illustrate how increasing nuclearity and incorporating heterometals expands the functional repertoire of iron-sulfur clusters, enabling substrate binding, redox tuning, and bifunctional catalysis. Importantly, these structural modifications allow such cofactors to mediate more complex transformations, including S-S bond cleavage and CO₂/CO interconversion. Therefore, we propose that increased nuclearity in iron-sulfur clusters enhances their structural diversity and equips them with adaptive strategies for catalytic engagement. This highlights the importance of further exploring the properties of these structurally complex and functionally versatile systems.

From a computational perspective, both cluster modelling and QM/MM simulations have proven indispensable in capturing key

intermediates, transition states, and transient oxidation states that are often elusive to experimental detection especially in complicated [FeS] cluster-dependent enzymes. These methods offer molecular-level insight into reactivity trends and guide rational enzyme engineering for environmental and synthetic applications.

Despite significant progress, several challenges remain. First, accurately modeling the influence of the protein environment, including long-range electrostatics, hydrogen bonding, and dynamic fluctuations, remains difficult, especially for large and flexible metalloclusters. Second, the complex electronic structures and spin-state diversity of iron–sulfur clusters often lead to near-degenerate states that are demanding to resolve with high precision. Third, reliable prediction of redox potentials, which are crucial for understanding electron transfer processes, continues to be challenging.

Moving forward, several promising directions can be anticipated. The development of more advanced quantum chemical methods with improved treatment of electron correlation and spin states, integration with enhanced sampling and polarizable force fields, and multiscale QM/MM dynamics will be essential to capture the full complexity of these catalytic systems. Additionally, better integration of experimental data (e.g., spectroscopy, crystallography, redox titrations) with computational models will enhance the accuracy and interpretability of theoretical predictions.

In summary, non-cubane [FeS] clusters represent a frontier in metalloenzyme catalysis, with their structural diversity, electronic tunability, and catalytic flexibility offering exciting opportunities for future biochemical discovery and synthetic design. Continued collaboration between experimental and theoretical efforts will be vital to fully harness the potential of these remarkable cofactors.

Acknowledgments

This work was financially supported by the National Natural Science Foundation of China (22173007).

References

- [1] Russell M.J., The alkaline solution to the emergence of life: energy, entropy and early evolution. *Acta Biotheor.*, **55** (2007), 133–179.
- [2] Ebrahimi K.H., Ciofi-Baffoni S., Hagedoorn P.L., Nicolet Y., Brun N.E.L., Hagen W.R. and Armstrong F.A., Iron-sulfur clusters as inhibitors and catalysts of viral replication. *Nat. Chem.*, 14 (2022), 253–266.
- [3] Sofia H.J., Chen G., Hetzler B.G., Reyes-Spindola J.F. and Miller N.E., Radical SAM, a novel protein superfamily linking unresolved steps in familiar biosynthetic pathways with radical mechanisms: functional characterization using new analysis and information visualization methods. *Nucleic Acids Res.*, 29 (2001), 1097–1106.
- [4] Beinert H., Holm R.H. and Munck E., Iron-sulfur clusters: nature's modular, multipurpose structures. *Science*, **277** (1997), 653–659.
- [5] Jeoung J.-H. and Dobbek H., Carbon dioxide activation at the ni, fe-cluster of anaerobic carbon monoxide dehydrogenase. *Science*, 318 (2007), 1461–1464.
- [6] Spatzal T., Aksoyoglu M., Zhang L.-M., Andrade S.L.A., Schleicher E., Weber S., Rees D.C. and Einsle O., Evidence

- for interstitial carbon in nitrogenase FeMo cofactor. *Science*, **334** (2011), 940.
- [7] Fontecilla-Camps J.C., Volbeda A., Cavazza C. and Nicolet Y., Structure/function relationships of [NiFe]- and [FeFe]hydrogenases. *Chem. Rev.*, 107 (2007), 4273–4303.
- [8] Lubitz W., Ogata H., Rudiger O. and Reijerse E., Hydrogenases. Chem. Rev., 114 (2014), 4081–4148.
- [9] Cracknell J.A., Vincent K.A. and Armstrong F.A., Enzymes as working or inspirational electrocatalysts for fuel cells and electrolysis. *Chem. Rev.*, 108 (2008), 2439–2461.
- [10] Lancey C., Tehseen M., Raducanu V.S., Rashid F., Merino N., Ragan T.J., Savva C.J., Zaher M.S., Shirbini A., Blanco F.J., Hamdan S.M. and Biasio A.D., Structure of the processive human pol δ holoenzyme. *Nat. Commun.*, 11 (2020), 1109–1120.
- [11] Crack J.C., Green J., Tomson A.J. and Le Brun N.E., Ironsulfur clusters as biological sensors: the chemistry of reactions with molecular oxygen and nitric oxide. *Acc. Chem. Res.*, 47 (2014), 3196–3205.
- [12] McCarthy E.L. and Booker S.J., Destruction and reformation of an iron-sulfur cluster during catalysis by lipoyl synthase. *Science*, **358** (2017), 373–377.
- [13] Wei W.-J. and Liao R.-Z., Mechanistic insights into the electron-transfer driven substrate activation by [4Fe-4S]-dependent enzymes. *ChemCatChem*, **16** (2024), e202301712.
- [14] Holm R.H. and Lo W., Structural conversions of synthetic and protein-bound iron-sulfur clusters. *Chem. Rev.*, **116** (2016), 13685–13713.
- [15] Mukherjee R.N., Stack T.D.P. and Holm R.H., Angle dependence of the properties of the [Fe₂X]⁴⁺ bridge unit (X = O, S): structures, antiferromagnetic coupling, and properties in solution. *J. Am. Chem. Soc.*, **110** (1988), 1850–1861.
- [16] Rao P.V. and Holm R.H., Synthetic analogues of the active sites of iron-sulfur proteins. *Chem. Rev.*, **104** (2004), 527– 559
- [17] Hagen K.S., Watson A.D. and Holm R.H., Synthetic routes to iron sulfide (Fe₂S₂, Fe₃S₄, Fe₄S₄, and Fe₆S₉), clusters from the common precursor [Fe(SC₂H₅)₄]²⁻): structures and properties of [Fe₃S₄(SR)₄]³⁻ and [Fe₆S₉(SC₂H₅)₂]⁴⁻), examples of the newest types of Fe-S-SR clusters. *J. Am. Chem. Soc.*, **105** (1983), 3905–3913.
- [18] L.-L.Tan, r. h. holm and s. c. lee, structural analysis of cubane-type iron clusters. *Polyhedron*, **58** (2013), 206–217.
- [19] Evans D.J., Garcia G., Santana M.D. and Torralba M.C., About the synthesis of the prismane [NEt₄]₂[Fe₆S₆I₆]. *Inorg. Chim. Acta*, **284** (1999), 296–299.
- [20] Christou G., Sabat M., Ibers J.A. and Holm R.H., A new structural type in iron-sulfide-thiolate chemistry: preparation, properties, and structure of the hexanuclear cluster [Fe₆S₉(Stert-C₄H₉)₂]⁴. *Inorg. Chem.*, 21 (1982), 3518–3526.
- [21] Deng L. and Holm R.H., Stabilization of fully reduced ironsulfur clusters by carbene ligation: the $[Fe_nS_n]^0$ oxidation levels (n = 4, 8). *J. Am. Chem. Soc.*, **130** (2008), 9878–9886.
- [22] Broderick J.B., Duffus B.R., Duschene K.S. and Shepard E.M., Radical S-adenosylmethionine enzymes. *Chem. Rev.*, **114** (2014), 4229–4317.
- [23] Castro L., Tórtora V., Mansilla S. and Radi R., Aconitases: non-redox iron-sulfur proteins sensitive to reactive species. *Acc. Chem. Res.*, **52** (2019), 2609–2619.

- [24] Crack J.C., Gray E. and Le Brun N.E., Sensing mechanisms of iron–sulfur cluster regulatory proteins elucidated using native mass spectrometry. *Dalton Trans.*, **50** (2021), 7887–7897.
- [25] Alfano M. and Cavazza C., Structure, function, and biosynthesis of nickel-dependent enzymes. *Protein Sci.*, 29 (2020), 1071–1089.
- [26] Fontecilla-Camps J.C., Volbeda A., Cavazza C. and Nicolet Y., Structure/function relationships of [NiFe]- and [FeFe]hydrogenases. *Chem. Rev.*, 107 (2007), 4273–4303.
- [27] Zahn L.E., Gannon P.M. and Rajakovich L.J., Iron-sulfur cluster-dependent enzymes and molybdenum-dependent reductases in the anaerobic metabolism of human gut microbes. *Metallomics*, **16** (2024), mfae049.
- [28] Kurisu G. and Tsukihara T., Forty years of the structure of plant-type ferredoxin. *J. Biochem.*, **171** (2022), 19–21.
- [29] Berkovitch F., Nicolet Y., Wan J.T., Jarrett J.T. and Drennan C.L., Crystal structure of biotin synthase, an Sadenosylmethionine-dependent radical enzyme. *Science*, 303 (2004), 76–79.
- [30] Barry S.M. and Challis G.L., Mechanism and catalytic diversity of rieske non-heme iron-dependent oxygenases. *ACS Catal.*, **3** (2013), 2362–2370.
- [31] Ferraro D.J., Gakhar L. and Ramaswam S., Rieske business: structure–function of rieske non-heme oxygenases. *Biochem. Biophys. Res. Commun.*, **338** (2005), 175–190.
- [32] Wagner T., Koch J., Ermler U. and Shima S., Methanogenic heterodisulfide reductase (HdrABC-MvhAGD) uses two noncubane [4Fe-4S] clusters for reduction. *Science*, **357** (2017), 699–703.
- [33] Dobbek H., Svetlitchnyi V., Gremer L., Huber R. and Meyer O., Crystal structure of a carbon monoxide dehydrogenase reveals a [Ni-4Fe-5S] cluster. *Science*, 293 (2001), 1281– 1285.
- [34] Jeoung J.-H., Fesseler J., Domnik L., Klemke F., Sinnreich M., Teutloff C. and Dobbek H., A morphing [4Fe-3S-nO]cluster within a carbon monoxide dehydrogenase scaffold. *Angew. Chem. Int. Ed.*, 61 (2022), e202117000.
- [35] Ohki Y., Imada M., Murata A., Sunada Y., Ohta S., Honda M., Sasamori T., Tokitoh N., Katada M. and Tatsumi K., Synthesis, structures, and electronic properties of [8Fe-7S] cluster complexes modeling the nitrogenase P-cluster. *J. Am. Chem. Soc.*, 131 (2009), 13168–13178.
- [36] Johnson D.C., Dean D.R., Smith A.D. and Johnson M.K., Structure, function, and formation of biological iron-sulfur clusters. *Annu. Rev. Biochem.*, 74 (2005), 247–281.
- [37] Pierrel F., Douki T., Fontecave M. and Atta M., MiaB protein is a bifunctional radical-S-adenosylmethionine enzyme involved in thiolation and methylation of tRNA. *J. Biol. Chem.*, **279** (2004), 47555–47563.
- [38] Landgraf B.J., Arcinas A.J., Lee K.H. and Booker S.J., Identification of an intermediate methyl carrier in the radical S-adenosylmethionine methylthiotransferases RimO and MiaB. J. Am. Chem. Soc., 135 (2013), 15404–15416.
- [39] Zhang B., Arcinas A.J., Radle M.I., Silakov A., Booker S.J. and Krebs C., First step in catalysis of the radical S-adenosylmethionine methylthiotransferase MiaB yields an intermediate with a [3Fe-4S]⁰-like auxiliary cluster. *J. Am. Chem. Soc.*, 142 (2020), 1911–1924.

- [40] Lotierzo M., Bui B.T.S., Leech H.K., Warren M.J., Marquet A. and Rigby S.E.J., Iron-sulfur cluster dynamics in biotin synthase: a new [2Fe-2S](1+) cluster. *Biochem. Biophys. Res. Commun.*, **381** (2009), 487–490.
- [41] Blomberg M.R.A., Borowski T., Himo F., Liao R.-Z. and Siegbahn P.E.M., Quantum chemical studies of mechanisms for metalloenzymes. *Chem. Rev.*, 114 (2014), 3601–3658.
- [42] Siegbahn P.E.M. and Himo F., The quantum chemical cluster approach for modeling enzyme reactions. *WIREs Comput. Mol. Sci.*, 1 (2011), 323–336.
- [43] Himo F. and de Visser S.P., Status report on the quantum chemical cluster approach for modeling enzyme reactions. *Commun. Chem.*, **5** (2022), 29.
- [44] Sheng X. and Himo F., The quantum chemical cluster approach in biocatalysis. *Acc. Chem. Res.*, **56** (2023), 938–947.
- [45] Siegbahn P.E.M. and Blomberg M.R.A., Transition-metal systems in biochemistry studied by high-accuracy quantum chemical methods. *Chem. Rev.*, **100** (2000), 421–438.
- [46] Warshel A. and Levitt M., Theoretical studies of enzymic reactions: dielectric, electrostatic and steric stabilization of the carbonium ion in the reaction of lysozyme. *J. Mol. Biol.*, 103 (1976), 227–249.
- [47] Siegbahn P.E.M. and Blomberg M.R.A., Quantum chemical studies of proton-coupled electron transfer in metalloenzymes. *Chem. Rev.*, **110** (2010), 7040–7061.
- [48] Tomasi J., Menucci B. and Cammi R., Quantum mechanical continuum solvation models. *Chem. Rev.*, 105 (2005), 2999– 3093.
- [49] Sun S.-Q. and Chen S.-L., An unprecedented ring-contraction mechanism in cobalamin-dependent radical S-adenosylmethionine enzymes. *J. Phys. Chem. Lett.*, **11** (2020), 6812–6818.
- [50] Zhao C., Li Y., Wang C. and Chen H., Mechanistic dichotomy in the activation of SAM by radical SAM enzymes: QM/MM modeling deciphers the determinant. ACS Catal., 10 (2020), 13245–13250.
- [51] Feng J.-Q., Shaik S. and Wang B.-J., Spin-regulated electron transfer and exchange-enhanced reactivity in Fe4S4-mediated redox reaction of the Dph2 enzyme during the biosynthesis of diphthamide. *Angew. Chem. Int. Ed.*, 60 (2021), 20430– 20436
- [52] Garcia-Viloca M., Gao J.-L., Karplus M. and Truhlar D.G., How enzymes work: analysis by modern rate theory and computer simulations. *Science*, 303 (2004), 186–195.
- [53] Dwyer M.A., Looger L.L. and Hellinga H.W., Computational design of a biologically active enzyme. *Science*, 304 (2004), 1967–1971.
- [54] Gallego J. and Varani G., Targeting RNA with small-molecule drugs: therapeutic promise and chemical challenges. *Acc. Chem. Res.*, **34** (2001), 836–843.
- [55] Himoa F. and Siegbahn P.E.M., Quantum chemical studies of radical-containing enzymes. *Chem. Rev.*, 103 (2003), 2421– 2456.
- [56] Noodleman L., Lovell T., Han W.-G., Li J. and Himo F., Quantum chemical studies of intermediates and reaction pathways in selected enzymes and catalytic synthetic systems. *Chem. Rev.*, 104 (2004), 459–508.
- [57] Shaik S., Cohen S., Wang Y., Chen H., Kumar D. and Thiel W., P450 enzymes: their structure, reactivity, and selectivity-

- modeled by QM/MM calculations. *Chem. Rev.*, **110** (2010), 949–1017.
- [58] Shaik S., Kumar D., De Visser S.P., Altun A. and Thiel W., Theoretical perspective on the structure and mechanism of cytochrome P450 enzymes. *Chem. Rev.*, 105 (2005), 2279– 2328.
- [59] Chung L.-W., Sameera W.M.C., Ramozzi R., Page A.J., Hatanaka M., Petrova G.P., Harris T.V., Li X., Ke Z., Liu F., Li H.-B., Ding L. and Morokuma K., The ONIOM method and its applications. *Chem. Rev.*, 115 (2015), 5678–5796.
- [60] Zhang T.-H., Zhang X.-Y. and Chung L.-W., Computational insights into the reaction mechanisms of nickel-catalyzed hydrofunctionalizations and nickel-dependent enzymes. *Asian J. Org. Chem.*, 7 (2018), 522–536.
- [61] Zhang X.-Y. and -W. Chung L., Alternative mechanistic strategy for enzyme catalysis in a ni-dependent lactate racemase (LarA): intermediate destabilization by the cofactor. *Chem. Eur. J.*, **23** (2017), 3623–3630.
- [62] Lai W.-Z., Li C.-S., Chen H. and Shaik S., Hydrogen-abstraction reactivity patterns from a to y: the valence bond way. *Angew. Chem. Int. Ed.*, **51** (2012), 5556–5578.
- [63] Wang C. and Chen H., . Convergent theoretical prediction of reactive oxidant structures in diiron arylamine oxygenases AurF and CmlI: peroxo or hydroperoxo? J. Am. Chem. Soc., 139 (2017), 13038–13046.
- [64] Lu J.-R., Lai W.-Z. and Chen H., C(sp³)-H hydroxylation in diiron β-hydroxylase CmlA transpires by amine-assisted O₂ activation avoiding Fe^{IV}₂O₂ species. *Angew. Chem. Int. Ed.*, 61 (2022), e202211843.
- [65] Yan X.-Y., Song J.-S., Lu Q.-Q. and -S. Li C., Mechanistic insights into the crucial roles of Glu76 residue in nickeldependent quercetin 2, 4-dioxygenase for quercetin oxidative degradation. J. Catal., 387 (2020), 73–83.
- [66] Lu Q.-Q., Song J.-S., Wu P., Li C.-S. and Thiel W., Mechanistic insights into the directing effect of Thr303 in ethanol oxidation by cytochrome P450 2E1. ACS Catal., 9 (2019), 4892–4901.
- [67] Fu Y.-H., Yu J., Fan F.-F., Wang B.-J. and Cao Z.-X., Elucidating the enzymatic mechanism of dihydrocoumarin degradation: insight into the functional evolution of methylparathion hydrolase from QM/MM and MM MD simulations. *J. Phys. Chem. B*, **128** (2024), 5567–5575.
- [68] Deng D., Jiang Z.-L., Kang L.-X., Liao L.-X., Zhang X.-D., Qiao Y.-B., Zhou Y., Yang L.-L., Wang B.-J. and Li A.-T., An efficient catalytic route in haem peroxygenases mediated by O2/small-molecule reductant pairs for sustainable applications. *Nat. Catal.*, 8 (2025), 20–32.
- [69] Fang C.-Y., Zhang L.-P., Wang Y.-C., Xiong W.-L., Yan Z.-E., Zhang W.-J., Zhang Q.-B., Wang B.-J., Zhu Y.-G. and Zhang C.-S., Discovery and biosynthesis of cihanmycins reveal cytochrome P450-catalyzed intramolecular C-O phenol coupling reactions. *J. Am. Chem. Soc.*, 146 (2024), 16478–16489.
- [70] Gan Z.-J., Feng J.-Q., Yin J.-B., Huang J.-P., Wang B.-J. and Zhang J.Z.-H., Diverse mechanisms for the aromatic hydroxylation: insights into the mechanisms of the coumarin hydroxylation by CYP2A6. ACS Catal., 14 (2024), 16277– 16286.
- [71] Wang Z.-F., Diao W.-W., Wu P., Li J.-F., Fu Y.-Z., Guo Z.-Y., Cao Z.-X., Shaik S. and Wang B.-J., How the

- conformational movement of the substrate drives the regioselective C–N bond formation in P450 TleB: insights from molecular dynamics simulations and quantum mechanical/molecular mechanical calculations. *J. Am. Chem. Soc.*, **145** (2023), 7252–7267.
- [72] Hou M.-J., Yuan J., Dong X.-Y., Wang Y.-J., Yang S.-H. and Gao J.-L., Engineering oxygen-independent NADH oxidase integrated with electrocatalytic FAD cofactor regeneration. *JACS Au*, 4 (2024), 3581–3592.
- [73] Liu N., Li L., Qin X., Li X., Xie Y.-X., Chen X.-H. and Gao J.-L., Theoretical insights into the generation mechanism of the Tyr122 radical catalyzed by intermediate X in class Ia ribonucleotide reductase. *Inorg. Chem.*, 62 (2023), 19498–19506.
- [74] Wang Y.-J., Dong L.-H., Su H. and Liu Y.-J., Dioxygen activation and nδ, nε-dihydroxylation mechanism involved in the formation of N-nitrosourea pharmacophore in streptozotocin catalyzed by nonheme diiron enzyme SznF. *Inorg. Chem.*, 61 (2022), 15721–15734.
- [75] Li H. and Liu Y.-J., Mechanistic investigation of isonitrile formation catalyzed by the nonheme Iron/α-KG-dependent decarboxylase (ScoE). ACS Catal., 10 (2020), 2942–2957.
- [76] Wang W., Qiu B. and Yang X.-Z., Computational prediction of pentadentate iron and cobalt complexes as a mimic of mono-iron hydrogenase for the hydrogenation of carbon dioxide to methanol. *Dalton Trans.*, 48 (2019), 8034–8038.
- [77] Karlsson A., Parales J.V., Parales R.E., Gibson D.T., Eklund H. and Ramaswamy S., Crystal structure of naphthalene dioxygenase: side-on binding of dioxygen to iron. *Science*, 299 (2003), 1039–1042.
- [78] Dhindwal S., Gomez-Gil L., Neau D.B., Pham T.T.M., Sylvestre M., Eltis L.D., Bolin J.T. and Kumar P., Structural basis of the enhanced pollutant-degrading capabilities of an engineered biphenyl dioxygenase. *J. Bacteriol.*, 198 (2016), 1499–1512.
- [79] Friemann R., Ivkovic-Jensen M.M., Lessner D.J., Yu C.-L., Gibson D.T., Parales R.E., Eklund H. and Ramaswamy S.R., Structural insight into the dioxygenation of nitroarene compounds: the crystal structure of nitrobenzene dioxygenase. *J. Mol. Biol.*, 348 (2005), 1139–1151.
- [80] Himo F., Recent trends in quantum chemical modeling of enzymatic reactions. *J. Am. Chem. Soc.*, **139** (2017), 6780–6786.
- [81] Himo F., Quantum chemical modeling of enzyme active sites and reaction mechanisms. *Theor. Chem. Acc.*, 116 (2006), 232–240
- [82] Becke A.D. and Density-functional thermochemistry. III. The role of exact exchange, . J. Chem. Phys., 98 (1993), 5648– 5652
- [83] Grimme S., Antony J., Ehrlich S. and Krieg H., A consistent and accurate ab initio parametrization of density functional dispersion correction (DFT-D) for the 94 elements H-Pu. *J. Chem. Phys.*, **132** (2010), 154104.
- [84] Zhao Y. and Truhlar D.G., The M06 suite of density functionals for main group thermochemistry, thermochemical kinetics, noncovalent interactions, excited states, and transition elements: two new functionals and systematic testing of four M06-class functionals and 12 other functionals. *Theor. Chem. Acc.*, **120** (2008), 215–241.

- [85] Perdew J.P., Density-functional approximation for the correlation energy of the inhomogeneous electron gas. *Phys. Rev. B*, **33** (1986), 8822.
- [86] Becke A.D., Density-functional exchange-energy approximation with correct asymptotic behavior. *Phys. Rev. A*, 38 (1988), 3098–3100.
- [87] Sousa S.F., Ribeiro A.J.M., Neves R.P.P., Bras N.F., Cerqueira N.M.F.S.A., Fernandes P.A. and Ramos M.J., Application of quantum mechanics/molecular mechanics methods in the study of enzymatic reaction mechanisms. WIRES Comput. Mol. Sci., 7 (2017), e1281.
- [88] Quesne M.G., Borowski T. and de Visser S.P., Quantum mechanics/molecular mechanics modeling of enzymatic processes: caveats and breakthroughs. *Chem. Eur. J.*, **22** (2016), 2562–2581.
- [89] Swiderek K., Tunon I. and Moliner V., Predicting enzymatic reactivity: from theory to design. WIREs Comput. Mol. Sci., 4 (2014), 407–421.
- [90] van der Kamp M.W. and Mulholland A.J., Combined quantum mechanics/molecular mechanics (QM/MM) methods in computational enzymology. *Biochemistry*, **52** (2013), 2708–2720.
- [91] Wang J., Wolf R.M., Caldwell J.W., Kollman P.A. and Case D.A., Development and testing of a general amber force field. *J. Comput. Chem.*, 25 (2004), 1157–1174.
- [92] Brooks B.R., Bruccoleri R.E., Olafson B.D., States D.J., Swaminathan S. and Karplus M., CHARMM: a program for macromolecular energy, minimization, and dynamics calculations. J. Comput. Chem., 4 (1983), 187–217.
- [93] Jorgensen W.L., Maxwell D.S. and Tirado-Rives J., Development and testing of the OPLS All-Atom force field on conformational energetics and properties of organic liquids. J. Am. Chem. Soc., 118 (1996), 11225–11236.
- [94] Kaminski G.A., Friesner R.A., Tirado-Rives J. and Jorgensen W.L., Evaluation and reparametrization of the OPLS-AA force field for proteins via comparison with accurate quantum chemical calculations on peptides. J. Phys. Chem. B, 105 (2001), 6474–6487.
- [95] Senn H.M. and Thiel W., QM/MM methods for biomolecular systems. Angew. Chem. Int. Ed., 48 (2009), 1198–1229.
- [96] Taylor A.M., Stoll S., Britt R.D. and Jarrett J.T., Reduction of the [2Fe–2S] cluster accompanies formation of the intermediate 9-mercaptodethiobiotin in escherichia coli biotin synthase. *Biochemistry*, 50 (2011), 7953–7963.
- [97] Challand M.R., Driesener R.C. and Roach P.L., Radical S-adenosylmethionine enzymes: mechanism, control and function. *Nat. Prod. Rep.*, 28 (2011), 1696–1721.
- [98] Kamachi T., Kouno T., Doitomi K. and Yoshizawa K., Generation of adenosyl radical from S-adenosylmethionine (SAM) in biotin synthase. J. Inorg. Biochem., 105 (2011), 850–857.
- [99] Broach R.B. and Jarrett J.T., Role of the [2Fe-2S]²⁺ cluster in biotin synthase: mutagenesis of the atypical metal ligand arginine 260. *Biochemistry*, **45** (2006), 14166–14174.
- [100] Fuchs M.G.G., Meyer F. and Ryde U., A combined computational and experimental investigation of the [2Fe–2S] cluster in biotin synthase. *J. Biol. Inorg. Chem.*, **15** (2010), 203–212.
- [101] Hanzelmann P. and Schindelin H., Binding of 5'-GTP to the C-terminal FeS cluster of the radical S-adenosylmethionine

- enzyme MoaA provides insights into its mechanism. *Proc. Natl. Acad. Sci.*, **103** (2006), 6829–6834.
- [102] Miller J.R., Busby R.W., Jordan S.W., Cheek J., Henshaw T.F., Ashley G.W., Broderick J.B., Cronan J.E. and Marletta J.M.A., Escherichia coli LipA is a lipoyl synthase: in vitro biosynthesis of lipoylated pyruvate dehydrogenase complex from octanoyl-acyl carrier protein. *Biochemistry*, 39 (2000), 15166–15178.
- [103] Yan F. and Fujimori D.G., RNA methylation by radical SAM enzymes RlmN and cfr proceeds via methylene transfer and hydride shift. *Proc. Natl. Acad. Sci.*, 108 (2011), 3930–3934.
- [104] Bassan A., Blomberg M.R.A., Borowski T. and Siegbahn P.E.M., Oxygen activation by rieske non-heme iron oxygenases, a theoretical insight. J. Phys. Chem. B, 108 (2004), 13031–13041.
- [105] Bassan A., Blomberg M.R.A. and Siegbahn P.E.M., A theoretical study of the cis-dihydroxylation mechanism in naphthalene 1, 2-dioxygenase. *J. Biol. Inorg. Chem.*, 9 (2004), 439–452.
- [106] Librando V. and Pappalardo M., Theoretical approach to the innovative mutation of naphthalene 1, 2-dioxygenase: a molecular dynamics and docking study. *J. Mol. Model.*, **20** (2014), 2354–2362.
- [107] Csizi K.S., Eckert L., Brunken C., Hofstetter T.B. and Reiher M., The apparently unreactive substrate facilitates the electron transfer for dioxygen activation in rieske dioxygenases. Chem. Eur. J., 28 (2022), e202103937.
- [108] Zhu L.-D., Zhou J., Zhang R.-M., Tang X.-W., Wang J.-J., Li Y.-W., Zhang Q.-Z. and Wang W.-X., Degradation mechanism of biphenyl and 4-4'-dichlorobiphenyl cis-dihydroxylation by non-heme 2, 3-dioxygenases BphA: a QM/MM approach. *Chemosphere*, 247 (2020), 125844–125856.
- [109] Hikaru S., W.Takahito, s. mika and f. kensuke, alteration of regiospecificity in biphenyl dioxygenase by active-site engineering. *J. Bacteriol.*, **184** (2022), 3682–3688.
- [110] Kensuke F., Hikaru S. and G.Masatoshi, Biphenyl dioxygenases: functional versatilities and directed evolution. *J. Bacteriol.*, 186 (2004), 5189–5196.
- [111] Gómez-Gil L., Kumar P., Barriault D., Bolin J.T., Sylvestre M. and Eltis L.D., Characterization of biphenyl dioxygenase of pandoraea pnomenusa B-356 as a potent polychlorinated biphenyl-degrading enzyme. *J. Bacteriol.*, **189** (2007), 5705–5715.
- [112] Brüning T., Thier R. and Bolt H.M., Nephrotoxicity and nephrocarcinogenicity of dinitrotoluene: new aspects to be considered. *Rev. Environ. Health*, **17** (2002), 163–172.
- [113] Pabis A., Geronimo I. and Paneth P., A DFT study of the cisdihydroxylation of nitroaromatic compounds catalyzed by nitrobenzene dioxygenase. *J. Phys. Chem. B*, **118** (2014), 3245–3256.
- [114] Wolfe M.D. and Lipscomb J.D., Hydrogen peroxide-coupled cis-diol formation catalyzed by naphthalene 1, 2-dioxygenase. *J. Biol. Chem.*, **278** (2003), 829–835.
- [115] Hedderich R., Berkessel A. and Thauer R.K., Purification and properties of heterodisulfide reductase from methanobacterium thermoautotrophicum (strain marburg). *Eur. J. Mol. Biol. Biochem.*, **193** (1990), 255–261.

- [116] Huang G.-F., Wagner T., Ermler U. and Shima S., Methanogenesis involves direct hydride transfer from H₂ to an organic substrate. *Nat. Chem. Rev.*, 4 (2020), 213–221.
- [117] Thauer R.K., The wolfe cycle comes full circle. *Proc. Natl. Acad. Sci.*, **109** (2012), 15084–15085.
- [118] Wu J. and Chen S.-L., Key piece in the wolfe cycle of methanogenesis: the S-S bond dissociation conducted by noncubane [Fe₄S₄] cluster-dependent heterodisulfide reductase. *ACS Catal.*, **12** (2022), 2606–2622.
- [119] Ragsdale S.W. and Pierce E., Acetogenesis and the Wood-Ljungdahl pathway of CO(2) fixation, biochim. biophys. acta. *Proteins Proteomics*, **1784** (2008), 1873–1898.
- [120] Siegbahn P.E.M., Energetics for CO₂ reduction by molybdenum-containing formate dehydrogenase. *J. Phys. Chem. B*, **126** (2022), 1728–1733.
- [121] Jormakka M., Tornroth S., Abramson J., Byrne B. and Iwata S., Purification and crystallization of the respiratory complex formate dehydrogenase-N from escherichia coli, acta crystallogr. Sect. D: Biol. Crystallogr., 58 (2002), 160–162.
- [122] Lindahl P.A., Ragsdale S.W. and Münck E., Mössbauer study of CO dehydrogenase from clostridium thermoaceticum. *J. Biol. Chem.*, **265** (1990), 3880–3888.
- [123] Amara P., Mouesca J.M., Volbeda A. and Fontecilla-Camps J.C., Carbon monoxide dehydrogenase reaction mechanism: a likely case of abnormal CO₂ insertion to a Ni-H(-) bond. *Inorg. Chem.*, **50** (2011), 1868–1878.
- [124] Fesseler J., Jeoung J.-H. and Dobbek H., How the [NiFe₄S₄] cluster of CO dehydrogenase activates CO₂ and NCO⁻. *Angew. Chem. Int. Ed.*, **54** (2015), 8560–8564.
- [125] Liao R.-Z. and Siegbahn P.E.M., Energetics for the mechanism of nickel-containing carbon monoxide dehydrogenase. *Inorg. Chem.*, **58** (2019), 7931–7938.
- [126] Heo J., Staples C.R. and Ludden P.W., Evidence for a ligand CO that is required for catalytic activity of CO dehydrogenase from rhodospirillum rubrum. *Biochemistry*, **40** (2001), 7604.
- [127] Kumar M., Lu W.P. and Ragsdale S.W., Binding of carbon disulfide to the site of Acetyl-CoA synthesis by the nickeliron-sulfur protein, carbon monoxide dehydrogenase. *from Clostridium thermoaceticum Biochemistry*, 33 (1994), 9769– 9777.
- [128] R. Breglia, F. Arrigoni, M. Sensi, C. Greco, P. Fantucci, L. D. Gioia and M. Bruschi, First-principles calculations on Ni,Fecontaining carbon monoxide dehydrogenases reveal key stereoelectronic features for binding and release of CO₂ to/from the C-cluster, Inorg. Chem., 60 (2021), 387–402.